Wind-Driven Dissolved Organic Matter Dynamics in a Chesapeake Bay Tidal Marsh-Estuary System

J. Blake Clark, [1]✉

Phone: 410-221-8313
Email: bclark@umces.edu

Wen Long, [2]

Maria Tzortziou, [3]

Patrick J. Neale, [4]

Raleigh R. Hood, [1]

[1] University of Maryland Center for Environmental Science, PO Box 775, Cambridge, MD, 21613 USA

[2] Pacific Northwest National Laboratory, 1100 Dexter Ave. North, Suite 400, Seattle, WA, 98109 USA

[3] The City College of New York, The City University of New York, 160 Convent Avenue, New York, NY, 10031 USA

[4] Smithsonian Environmental Research Center, PO Box 28, Edgewater, MD, 21037 USA

Abstract

Controls on organic matter cycling across the tidal wetland-estuary interface have proved elusive, but high-resolution observations coupled with process-based modeling can be a powerful methodology to address shortcomings in either methodology alone. In this study, detailed

observations and three-dimensional hydrodynamic modeling are used to examine biogeochemical exchanges in the marsh-estuary system of the Rhode River, MD, USA. Analysis of observations near the marsh in 2015 reveals a strong relationship between marsh creek salinity and dissolved organic matter fluorescence (*fDOM*), with wind velocity indirectly driving large amplitude variation of both salinity and *fDOM* at certain times of the year. Three-dimensional model results from the Finite Volume Community Ocean Model implemented for the wetland system with a new marsh grass drag module are consistent with observations, simulating sub-tidal variability of marsh creek salinity. The model results exhibit an interaction between wind-driven variation in surface elevation and flow velocity at the marsh creek, with northerly winds driving increased freshwater signal and discharge out of the modeled wetland during precipitation events. Wind setup of a water surface elevation gradient axially along the estuary drives the modeled local sub-tidal flow and thus salinity variability. On sub-tidal time scales (>36 h, <1 week), wind is important in mediating dissolved organic matter releases from the Kirkpatrick Marsh into the Rhode River.

Keywords

Tidal wetlands
Chesapeake Bay
Hydrology
Dissolved organic matter
FVCOM

Communicated by Mark J. Brush

Electronic supplementary material

The online version of this article (doi: 10.1007/s12237-017-0295-1) contains supplementary material, which is available to authorized users.

Introduction

Wetlands can be important buffers for coastal flooding and storms (Haddad

et al. 2016), and they provide habitat and nursery grounds for many species of animals that have cultural and economic significance, including birds, fish, mammals, and invertebrates. In addition to more tangible ecosystem services, the generally high productivity of tidal wetlands makes them dynamic carbon fixers and transformers of organic material, playing a potentially substantial role in the coastal carbon cycle. In the face of rising seas and warming coastal oceans, interest in marsh biogeochemistry and the ecosystem services and carbon cycling associated with them has been increasing.

Numerous studies have quantified the fluxes of materials between tidal wetlands and adjacent estuaries on varying time scales (e.g., Teal 1962; Nixon 1980; Dame et al. 1991; Childers et al. 1993; Tzortziou et al. 2008). Brackish and salt marshes have high rates of primary production, generally being net carbon sinks from the atmosphere (Chmura et al. 2003; Bridgham et al. 2006), while also contributing a large source of dissolved inorganic carbon and dissolved organic matter (DIC and DOM) to the coastal ocean (Wang and Cai 2004; Herrmann et al. 2015). A recent estimate of a tidal wetland organic carbon flux of 1.2–2.5 Tg C $year^{-1}$ to the eastern coastal waters of the USA indicates tidal wetlands play an important role in the coastal carbon cycle (Herrmann et al. 2015). Within the bulk DOM pool produced by marshes, there are significant amounts of chromophoric DOM (CDOM; Tzortziou et al. 2008; Tzortziou et al. 2011). CDOM is an important water quality optical constituent that makes up a substantial portion of the ultraviolet light-absorbing capacity of optically complex estuarine and coastal waters (Del Vecchio and Blough 2002; Twardowski et al. 2004; Sulzberger and Durisch-Kaiser 2009). Marsh-derived CDOM has been shown to be highly photolabile (Moran et al. 2000; Miller et al. 2002; Tzortziou et al. 2007) and studies in the Chesapeake Bay show that it is also optically and chemically distinctive (i.e., more humic and more strongly absorbing) compared to CDOM from other terrestrial sources (Lu et al. 2013; Tzortziou et al. 2008). Furthermore, DOM fluorescence (*fDOM*) has been strongly linked to wetland-derived dissolved organic carbon (DOC) fluxes with both *fDOM* and DOC concentration having a strong tidal component peaking around low tide (Tzortziou et al. 2008).

AQ1

AQ2

In addition, marsh carbon fixation and processing have widespread implications for net ecosystem production of the east coast of North America and in particular Chesapeake Bay (Herrmann et al. 2015). Wetlands make up 1% of the total watershed in the mid-Atlantic Bight but contribute up to 40% of the total organic carbon export into estuarine and coastal waters (Herrmann et al. 2015). Marsh-estuary dissolved organic matter (DOM) fluxes have been studied extensively for over 30 years, with most studies showing that coastal marshes are strong sources of dissolved organic carbon and nitrogen to adjacent waters (e.g., Dame et al. 1986; Childers et al. 1993; Tzortziou et al. 2008). However, generalizations about the magnitude of these fluxes and the factors that drive their spatiotemporal variability have proven elusive.

Wetland inundation regimes and water flux exert substantial control over many biogeochemical processes in marsh-estuary systems (Fagherazzi et al. 2013). Factors that influence marsh water intrusion on temporal scales longer than tidal cycles can have potentially important implications in microtidal environments such as Chesapeake Bay. In Chesapeake Bay, variations in freshwater discharge (Schubel and Pritchard 1986) and wind speed (e.g., Blumberg and Goodrich 1990; Scully et al. 2005) can both have a strong influence on the residual flow patterns of the Bay. Wind also affects flushing, residence time, and salinity variability in shallow water estuaries (Geyer 1996). It is therefore not surprising that wind forcing also impacts biogeochemical fluxes associated with marsh ecosystems. For example, Childers et al. (1993) reported that salt marshes in coastal Georgia have varying inorganic nutrient flux responses associated with changes in wind direction and wave height at exposed marsh sites, and that more exposed marshes have higher amounts of potentially wind-driven DOM exchange. Sub-tidal inundation variation in tidal wetlands has also been linked to wind forcing (Dame et al. 1986; Childers et al. 1993; Bockelmann et al. 2002), but sub-tidal flow variability has yet to be quantitatively linked to DOM transport across the wetland-estuary interface. Implementing high-resolution monitoring programs that can capture transient wind and storm events associated with marsh-estuary fluxes is challenging, partly due to high

human resource and material costs in addition to high spatial and temporal heterogeneity associated with intertidal wetlands (Jordan and Correll 1991). The advent of in situ optical sensors that can measure various water column properties including *fDOM* has made high-frequency observations much more attainable. Furthermore, modeling combined with the in situ sensing technology can offer insights into the spatiotemporal variability of marsh-estuary coupled water flow with high resolution over a wide range of scales. **AQ3**

Biogeochemical degradation, physical transport and mixing, and photochemical transformations all contribute to the distribution of DOM in estuarine waters. The highly variable tidal signal inherently influences the biogeochemical processes that occur as wetland DOM is advected between the wetland and estuary. This study addresses the processes of physical mixing and transport to examine the influence they have on the observed temporal patterns of DOM variability at the wetland creek. Specifically, a combination of observations and modeling is used to investigate how wind influences the outflow of DOM from the Kirkpatrick Marsh into the Rhode River in Chesapeake Bay, USA. First, an instrument deployment at the marsh creek is used to provide insight into the temporal variability of salinity and *fDOM*. Insight gained from the instrument deployment is then used to inform numerical experiments utilizing a Rhode River implementation of the Finite Volume Community Ocean Model (RhodeFVCOM). Specifically, RhodeFVCOM is used to examine how wind velocity influences the temporal and spatial salinity and flow variability. These experiments reveal that wind forcing affects inundation timing and extent and significantly alter marsh creek flow velocity, with northerly winds enhancing marsh water efflux. The results of this numerical study, in conjunction with the observational data set, demonstrate that wind largely controls water advection and inundation in the marsh and sub-tidal hydrological variability and thus controls marsh-estuary DOM exchange.

Methods

Site Description and Observations

The Rhode River, MD, USA is a shallow water tributary located on the

western shore of Chesapeake Bay just south of Annapolis, MD (Fig. 1a, b). The Kirkpatrick Marsh is a fully developed mesohaline (0–14 psu) marsh that is located near the head of the Rhode River at 38°52′30″N, 76°32′50″W (Fig. 1c). The bathymetry in the Rhode River slopes from a depth of approximately 0.3 m at the marsh edge to 4 m at the mouth of the river.

Fig. 1

a Chesapeake Bay with the **b** RhodeFVCOM model domain, and **c** the Kirkpatrick Marsh area in the RhodeFVCOM model domain. *Stars* represent freshwater discharge points and the *dot* represents the marsh element used in marsh hydrology analysis. The Kirkpatrick Marsh is outlined in **c**, and measurements were taken at the marsh creek and SERC, indicated by the *arrows*

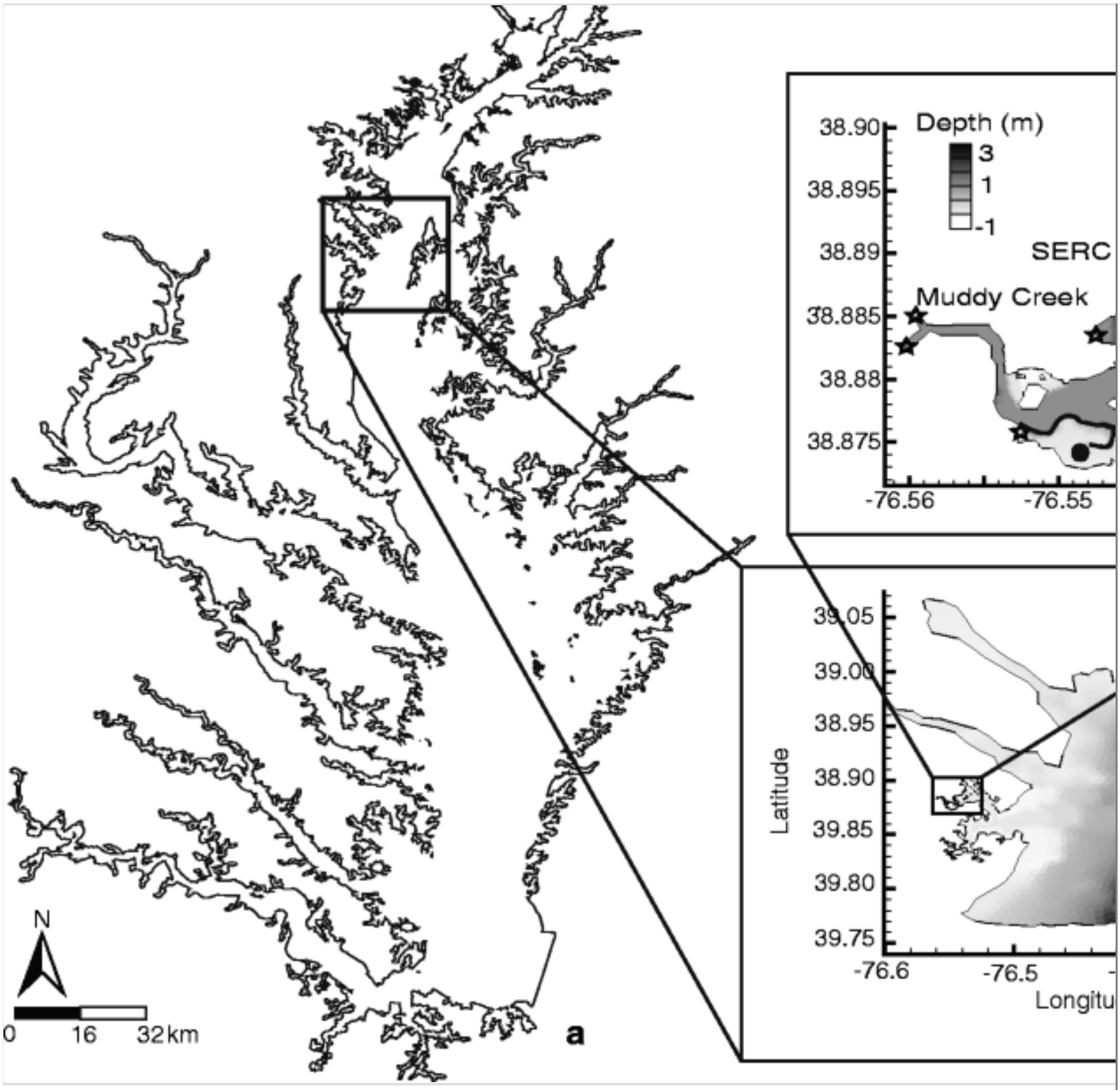

The largest input of freshwater into the estuary is from Muddy Creek (Fig. 1c), with a maximum instantaneous discharge of 15 m^3 s^{-1} and a median daily discharge of 0.13 m^3 s^{-1} in the modeled year 2005 (Breitburg et al. 2008). Marsh plant community density in the Kirkpatrick Marsh ranges from 200 to 1000 plants m^{-2} with substantial inter-annual variability (Rasse et al. 2005). *Schoenoplectus americanus* makes up a significant portion of the plant community and average high marsh plant diameter at an adjacent marsh measured 3.75 mm (Ikegami et al. 2006). Among other species commonly found in brackish marshes, there are stands of *Spartina patens* in areas with higher elevation (Jordan and Correll 1991). The portion of the Kirkpatrick

Marsh under study is mainly flushed by a tidal creek outfitted with a flow-through flume that is the main conduit linking ~3 ha of marsh area to the Rhode River (Jordan and Correll 1991).

A multiparameter EXO2 6-port water quality sonde (Yellow Springs Instruments, YSI) was deployed at the Kirkpatrick Marsh creek starting in November 2014 and sampling nearly continuously through 2015. Measurements included salinity, temperature, *chl a* fluorescence, dissolved oxygen, DOM fluorescence (*fDOM*), and pH at 15-min intervals 0.25 m above the marsh creek sediment. A similarly configured instrument was operated at the Smithsonian Environmental Research Center (SERC) dock (38°53′8″N, 76°32′30″W) which is about 1 km downstream of the marsh in the Rhode River (Fig. 1c). Both instruments are outfitted with an automatic wiper that cleans the active surface of all probes, allowing for less maintenance and longer deployment times. The probes were regularly inspected for bio-film accumulation, and the instrument was cleaned and calibrated before and after each deployment. Deployment periods between calibrations in the summer were around 2 weeks, longer during cool weather. *fDOM* data have been corrected for the effects of turbidity and temperature-dependent variation in quantum yield (cf. Downing et al. 2012).

A SonTek-IQ acoustic doppler velocimetry (ADV) probe was intermittently deployed at the marsh creek flume beginning June 2015 to measure current velocity and depth at 5 cm above the marsh creek sediment surface. The ADV sampled for a 120-s period every 5 min, averaging the measured velocity and depth over the sample period. Flow measurements obtained at 15 min intervals over a 55-day ADV deployment in the summer were used to generate a hypsometric relationship for area inundated for a given tidal stage. The flow data obtained was used to compare the calculated wetland inundation with the model predicted wetland inundation. In addition, a deployment in November 2015 is used for a comparison between model dynamics and observed velocity at the marsh creek.

Model Development and Implementation

The Finite Volume Community Ocean Model (FVCOM, Chen et al. 2003)

was implemented for a section of mid Chesapeake Bay including the Rhode River and Kirkpatrick Marsh (Fig. 1b) to analyze controls on hydrodynamic processes in the marsh and the estuary downstream. The wetting and drying treatment of intertidal areas available in FVCOM gives an accurate representation of intertidal hydrodynamics in a wetland-estuarine system in the Satilla River, GA (Chen et al. 2008), and was therefore selected for this application.

The model domain includes two main stem EPA Chesapeake Bay Program (CBP) long-term water quality model stations as well as four stations on the east and west shoals of the bay (Fig. 1b). The northern open boundary of the model domain is near the Chesapeake Bay Bridge, and the southern open boundary is just north of Poplar Island. The near-continuous measurements of temperature and salinity at the SERC dock allowed for shallow water model validation (see “Results”).

Eight freshwater discharge sites were included in the model domain, four of which are adjacent to the Kirkpatrick Marsh (stars in Fig. 1c). Measured freshwater discharge from the three V-notch weirs (Breitburg et al. 2008) in the Rhode River watershed was extrapolated to the other five discharge points by normalizing the flow measured at the weir to watershed area. When a flow meter records low or no flow over a long period of time and a sudden increase in discharge occurs, the flow recorders miss the initial increase in discharge. In order to prevent an over-estimate of flow into the model domain, an algorithm was employed to account for the missed flow when doing a linear temporal interpolation (Jordan, personal communication). When there is a sharp increase in flow after extended low flow periods, the algorithm assumes a constant flow rate until the sharp increase in flow is observed.

A nested model approach is used to force the northern and southern open boundaries with temperature, salinity, and sea surface height (SSH). Time series of SSH at the open boundaries were extracted at hourly intervals from a solution of a larger-scale FVCOM simulation developed for this study to drive the RhodeFVCOM tidal forcing. A model solution for daily temperature and salinity was taken at daily intervals from the Chesapeake

Bay Regional Ocean Modeling System (ChesROMS; Xu et al. 2012) grid points closest to the RhodeFVCOM north and south open boundaries. Two- and three-dimensional interpolations were done for SSH, temperature, and salinity onto the RhodeFVCOM open boundaries. Lastly, the spatially interpolated temperature and salinity from ChesROMS were linearly interpolated in time from a daily output to the hourly time step and used to force RhodeFVCOM.

The estuarine surface boundary is forced using North American Regional Reanalysis (NARR) model output for the year 2005 (http://rda.ucar.edu /datasets/ds608.0/). Three-hourly NARR data from the NARR grid cell that covers the majority of the RhodeFVCOM domain was applied uniformly over the entire model domain. Wind speed *u* and *v* vector components at 10 m above sea surface were used to calculate surface wind stress in the model (formulated from Large and Pond 1981). Temperature at 10 m above sea level, surface pressure (Pa), and relative humidity (%) at 2 m above sea level, along with the NARR wind and model calculated sea surface temperature (SST, °C), were used to compute the sensible and latent heat flux in the model internally using the COARE 2.6 algorithm (Fairall et al. 1996). This method allowed a dynamic feedback between the model predicted SST and the heat flux calculation. Net short-wave and long-wave radiation from NARR was used to close the heat flux calculation internally. A correction factor of 0.5 was applied to the NARR estimated net long-wave radiation flux in order to resolve the temperature in the summer and partially account for systematic over prediction of long-wave radiation flux (Kumar and Merwade 2011).

Model horizontal resolution increases from ~400 m in the main channel portion of Chesapeake Bay to less than 10 m in the marsh area. The high spatial resolution is necessary to attempt to resolve bathymetric features within the marsh. The unstructured mesh contains 8138 nodes and 14,572 elements. Rhode River bathymetry was input manually into the Surface Water Modeling System (SMS) mesh generation software package (SMS version 8.0, AQUAVEO) from NOAA chart #12270 (www.charts.noaa.gov) and interpolated to the nodes of the model grid.

FVCOM uses a vertical hybrid terrain following coordinate system commonly referred to as sigma coordinates. In areas with still-water depth less than 3 m, the vertical coordinates form an exponential distribution with decreasing resolution with depth. In areas with depth greater than 3 m, the vertical coordinates change to a parabolic distribution with coarser vertical resolution in the middle of the water column. This is implemented to counteract spurious heating and cooling in the surface layers of the shallow areas of the model, while resolving boundary layer effects in deeper regions.

A marsh plant momentum sink ~~was~~is included in the model (Wang et al. 2014) in order to simulate the drag imposed by marsh grass on the tidal water flowing through the marsh. Following Nepf (1999), the momentum sink calculates the drag imposed by a rigid cylindrical body and subtracts it from the momentum equation solved for each grid cell in the water column. Eq. 1 (Wang et al. 2014) is used to numerically solve for the drag force on the flow due to the presence of marsh grass in a spatially explicit context, where F^{M} is the momentum sink due to drag (m s^{-2}), N is the number of plants in the marsh element, C_d is the drag coefficient (dimensionless), A is the cross-sectional area of plant stems (Diameter x Height, m^2), V_C is the element volume (m^3), and u is the velocity of the water at the element centroid (m s^{-1}).

$$F^{M} = \frac{1}{2}\frac{NC_dA}{V_C}|\vec{u}|\,\vec{u} \qquad 1$$

An average stem number density of 600 plants m^{-2} (Rasse et al. 2005) and a stem diameter of 3.75 mm (Ikegami et al. 2006) were used to calculate a cross-sectional area of influence in each cell specified upon model startup as containing marsh plants. Table 1 summarizes the marsh plant drag model parameterization.

Table 1

Parameters tuned for salinity, temperature, and marsh plant drag properties

Parameter	Description	Value

Parameter	Description	Value
VPRNU	Vertical Prandtl number	1.00
HPRNU	Horizontal Prandtl number	1.00
UMOL	Molecular diffusivity ($m^2\ s^{-1}$)	10^{-6}
HORCON	Horizontal diffusion coeff. ($m^2\ s^{-1}$)	2.00
B_{FRIC}	Bottom friction	0.002
N	Marsh plant stem density (m^{-2})	600
D	Marsh plant stem diameter (mm)	3.75
C_D	Marsh plant drag coefficient	0.005

In FVCOM, a minimum depth (D_{min}) is required to maintain computational logic in the intertidal zone for the wetting and drying scheme (Chen et al. 2013). The minimum depth is the modeled water elevation where “dry” conditions take place and calculations for temperature and salinity diffusion cease until D_{min} is exceeded. A D_{min} value of 0.05 m was used in this research for model stability purposes.

The boundaries of the marsh areas were extracted from traced paths in Google Earth (GoogleEarth 7.1.5). The mode-split time stepping scheme of FVCOM requires a small external mode (barotropic) to internal mode (baroclinic) time step ratio when grid resolution is fine and intertidal areas are shallow (see Chen et al. 2013 for intertidal tests and numerical constraints). Therefore, an external time step (DTE) of 2 s and internal time step (DTI) of 6 s were used. The computations were carried out using OpenMPI on an 8 core 2014 Mac Pro, which took approximately 2 days in wall clock time for 242 model days.

Model Numerical Experiments

Model parameter optimization tests were carried out to find the best parameter set for predicting salinity and temperature in the Rhode River. The parameter set that produced the best results was used as the control run for

the numerical experiments (Table 1). The bottom friction (B_{FRIC}) and horizontal diffusion coefficient (HORCON) were the most important parameters affecting salinity and SSH in the Rhode River. Temperature variation was strongly dependent on the surface forcing and the vertical layer distribution in the modeled water column. In order to find out how wind velocity affected the system, two model "experiments" with varying atmospheric forcing were carried out in addition to a control run. Observations at the Kirkpatrick Marsh creek in 2015 suggested a non-linear relationship between wind forcing and salinity. To explore this relationship, numerical experiments were set up to test how the model replicated the observed non-linear interactions at different times of the year.

Test B is the baseline model run (the control). Tests SW and NW were set up so that southerly (Test SW) and northerly (Test NW) winds blow for a 48-h bracket (±24 h) around storm events. Storm events were defined as an increase in total discharge of 0.25 $m^3\ s^{-1}$ into the entire Muddy Creek watershed over a 15-min time period, totaling 12 events. Wind climatologies from Baltimore-Washington Airport, MD from 2010 through 2013 reveal that, in general, winds are stronger and from a more northwesterly direction in autumn, winter and spring (Vinnikov 2015; http://www.atmos.umd.edu /~kostya/NIST/WIND/SURFACE/KBWI_2010_13_WIND_2.pdf). In the summer, winds tend to be of smaller magnitude and the direction switches to having a more pronounced southerly component. The 2-day wind bracket in the model was designed to capture any potential lag influences associated with salinity intrusion, flow velocity, and wind speed.
AQ4

The model initial condition was set using output from a previous baseline model run ending March 31, 2005 and run recursively three times for the entire year. The numerical experiments were conducted beginning March 31, 2005 running 242 days through November 30, 2005. The model time period captured the spring freshet in 2005 that peaked in mid-April. Hydrodynamic parameters were adjusted in order to minimize model temperature and salinity solution error at the SERC dock (Table 1).

Statistical Analysis

Time series comparisons of root mean square error (RMSE) and correlation coefficient (*r*) characterized model skill for temperature and salinity (Stow et al. 2009). A low frequency pass cutoff filter MATLAB function (*lpfilt;* Sherwood 1989; MATLAB Version R2014B, The Mathworks Inc.) was used to remove the tidal signal from both the observed (salinity, *fDOM*, depth, wind velocity) and the modeled (salinity, flow velocity, and SSH) time series in order to examine the response of the sub-tidal variability to the effect of wind. This algorithm employs a fast Fourier transform (fft) and tapered moving box-car algorithm to filter both modeled and observed time series in the frequency domain before statistical analysis. Non-stationary time series were detrended by removing the best-fit least-squares regression line of the data from the total data set. Cross-covariance analysis of the three observed time series was conducted to assess covariance of *fDOM*, salinity, wind velocity, and depth.

AQ5

Equation 2 is used to calculate the area of inundated marsh at the Kirkpatrick Marsh creek where AI is the area inundated of the marsh (m^2), V_F is the flow velocity at the marsh flume ($m\ s^{-1}$), A_F is the cross-sectional area

$$\mathrm{AI} = \frac{V_F A_F}{\frac{dZ}{dt}} \qquad 2$$

of the marsh flume (m^2), and *dZ/dt* is the temporal derivative of the tidal height ($m\ s^{-1}$). The hypsometry of a wetland is based on the relationship between flooding or ebbing water flow across a known cross-sectional area and marsh tidal inundation rate of change. If the discharge through the flume is known, then the area flooded within the marsh can be inferred using Eq. 2. RhodeFVCOM predicted total, instantaneous area inundated combined with the observed area inundated calculated from the hypsometric relationship allows an indirect but useful comparison of the model and the Kirkpatrick Marsh. For the hypsometry analysis, only flood tides where the change in tidal height, dZ, was greater than 0.01 m were used to eliminate noise associated with low or no flow (Jordan and Correll 1991).

Augmented Dickey-Fuller tests (ADF) conducted using the R statistical software (version 3.1; R Core Team, 2015) library "tseries" (version 0.10–34; Trapletti and Hornik 2015) function *adftest* were used to assess the stationarity and potential cointegration of the detrended, low-pass filtered time series of *fDOM*, salinity, and observed wind velocity components. *fDOM* and salinity were filtered at a 36-h cutoff, while wind components were filtered at a 24-h cutoff to remove diel periodicity. The ADF tests accepted the alternative hypothesis of unit root of 0 of N-S and E-W wind ($p < 0.05$) for all time periods except fall E-W wind (Table 2). Therefore, analysis between wind and *fDOM* avoided the potential spurious relationship of cointegration among variables that could produce dubious correlations. ADF tests of salinity failed to reject the null hypothesis of non-stationarity in the spring but accepted the alternative of stationarity in the summer and fall. In the analysis, westerly and southerly winds are defined as positive (positive *u* and *v* vector components).

Table 2

Augmented Dickey-Fuller (ADF) test results and associated *p* values for the four variables used in the covariance analysis. If *p* is less than 0.05, the alternative hypothesis was accepted with 95% confidence of unit root 0 and thus the time series are stationary

Property	Spring ADF, *P*	Summer	Fall
Salinity	−1.76, 0.68	−3.99, <0.01	−3.52, 0.04
fDOM	−3.18, 0.09	−4.83, <0.01	−2.83, 0.23
NS Wind	−4.09, 0.02	−3.79, 0.02	−3.74, 0.02
EW Wind	−3.64, 0.03	−5.74, <0.01	−2.83, 0.23

Results

Observations

Observed wind data from Tolchester Beach, MD (NOAA Tides and Currents; tidesandcurrents.-noaa.gov) showed an alternating wind pattern

corresponding to the sub-tidal variability of salinity and *fDOM* at the marsh creek in 2015 (Fig. 2). Covariance of salinity and *fDOM* at the marsh creek appeared to have a seasonal component with strong negative covariance in the spring and fall at a lag centered around 0.5 days following changes in wind direction (Fig. 3a, c). Southerly and easterly wind components were anti-correlated with the *fDOM* signal while northerly and westerly wind components were positively correlated with the *fDOM* signal (Table 3). *fDOM* lagged changes in the peak N-S wind velocity components by 9–10 h and the peak E-W wind velocity components by 12–22 h consistently across the three seasons. Wind velocity and *fDOM* had a greater coefficient of covariance in the spring and fall relative to the summer for both N-S and E-W wind components. This was likely driven by high wind speeds that were sustained for longer periods in both component directions during spring and fall. The seasonal variability in wind direction and speed is relatively consistent with a wind climatology from Baltimore-Washington International Airport, MD which is ~40 km away (Vinnikov 2015).

Fig. 2

Low-pass cutoff filtered (36 h frequency) salinity and DOM fluorescence (*fDOM)* observed at the Kirkpatrick Marsh creek in **a** spring, **b** summer, and **c** fall in 2015. The stick plots are the observed hourly wind speed at Tolchester Beach, MD (NOAA Tides and Currents; tidesandcurrents.noaa.gov). *Black dots* indicate days when greater than 3 mm of rain fell at Annapolis, MD (~~weatherunderground.com~~Weather Underground; www.weatherunderground.com)

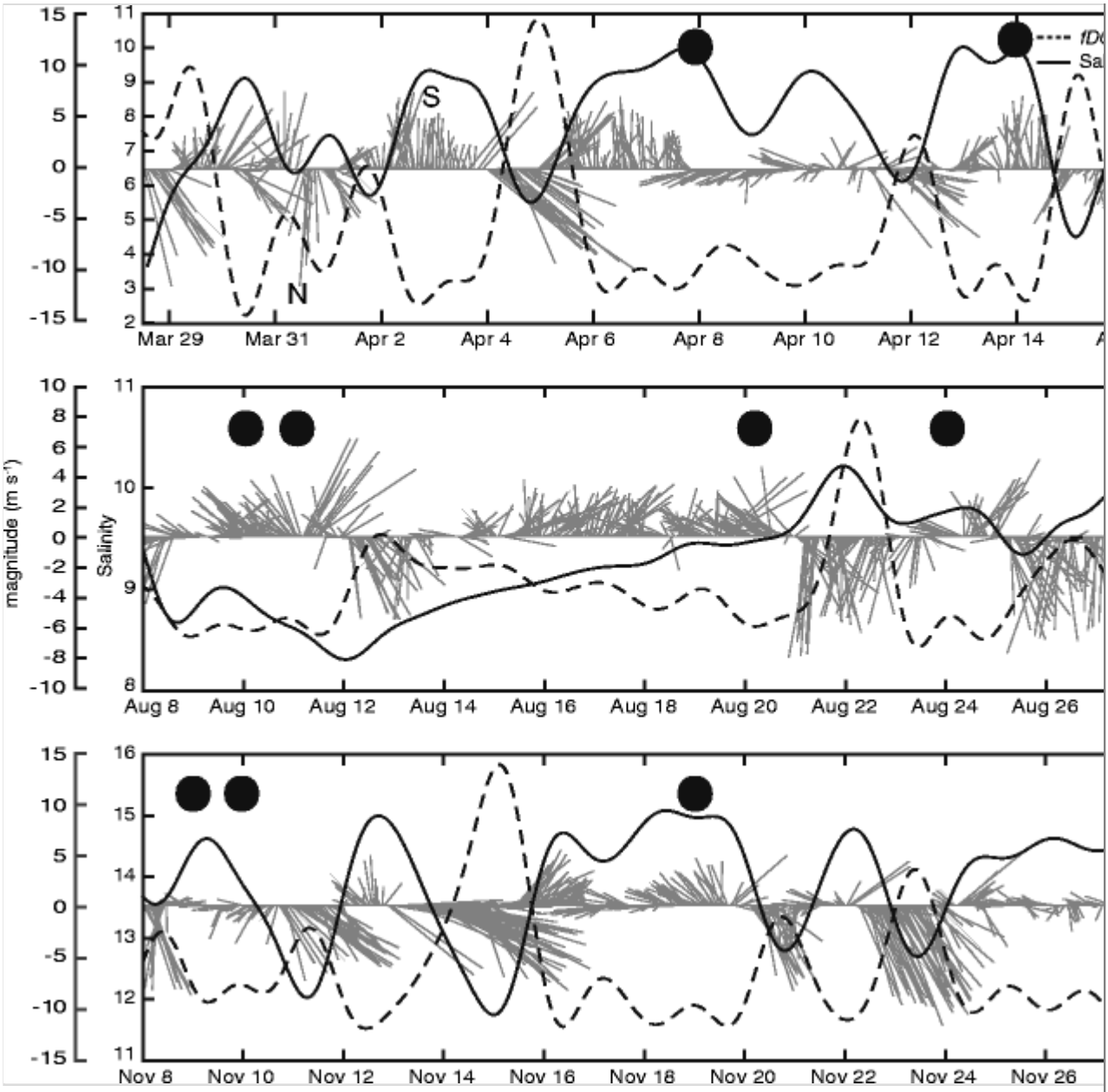

Fig. 3

Cross-covariance of North-South (NS) winds, East-West (EW) winds, and salinity with *fDOM* at the Kirkpatrick Marsh creek for the three time periods in Fig. 2. Southerly wind (v) and westerly wind (u) are defined as positive. Lags at the maximum absolute covariances are given in Table 3

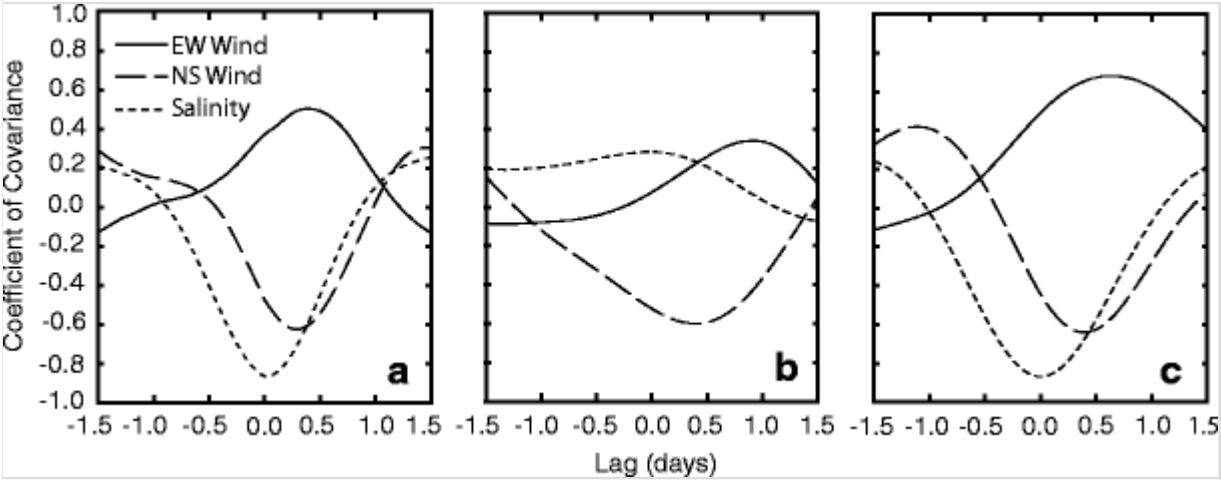

Table 3

Lag (h) at minimum or maximum absolute covariance and the associated coefficient of covariance of observed *fDOM* and wind, salinity, and depth for the three observational periods shown in Fig. 2 and for the entire observational record (Total). A complete depth record was not available to coincide with the other measurements

Property	Spring lag, *r*	Summer	Fall	Total
NS Wind	10, −0.74	10, −0.64	10, −0.66	9, −0.37
EW Wind	12, 0.66	22, 0.31	16, 0.69	18, 0.36
Salinity	1, −0.81	245, −0.20	0, −0.87	3, −0.55
Depth	1, −0.66	2–0.76	1, −0.75	~~=2, =0.09~~

In the summer, N-S wind velocity exhibited covariance with *fDOM* (r = 0.60) as in spring and fall while E-W winds exhibited less covariance with a longer lag than the other two observation periods (r = 0.34). The lower relative importance of the E-W wind component in the summer is likely due to a lack of a strong E-W wind event. The higher positive covariance in the N-W wind direction with *fDOM* appears to be due to the sustained low-speed southerly wind during 14–20 August coinciding with a steadily decreasing trend in *fDOM* signal and an increase in salinity (Fig. 2b). In addition, a strong wind event coinciding with the largest release of *fDOM* in the time series occurred on August 22. Wind patterns also differed

across seasons; in the spring and fall, there was oscillatory behavior of component wind vectors with strong northwest winds followed by lower wind magnitude from a generally southerly direction (Fig. 2a, c). The magnitude of summer wind was lower, on average, with the aforementioned long period of sustained light southerly winds in mid-August, which also coincided with a steady increase in marsh creek salinity.

Low-pass filtered depth and *fDOM* were consistently correlated, with a strong negative covariance across all seasons (Table 3, Fig. 4a). The high correlation and similar lag between depth and salinity and *fDOM* indicate that the primary control on the flux of water between the marsh and estuary was the SSH at the marsh creek and the marsh inundation, which was influenced by wind on sub-tidal time scales. As the marsh was flooded (high depth), *fDOM* was low due to the presence of primarily estuarine water at the marsh creek. As the marsh drained and SSH dropped due to sustained northwesterly winds, high-*fDOM* marsh water was released from the wetland into the estuary, evidenced by the consistently strong *fDOM* signal at low water depths (Fig. 4a). This relationship is also indicated by cross-plots of salinity and *fDOM* (Fig. 4b), although there is substantial variability across seasons. The lack of a strong relationship between *fDOM* and salinity in the summer is clearly shown by the summer scatter plot of salinity and *fDOM* (Fig. 4b). There also appeared to be two sources of *fDOM*, particularly in the fall, which is indicated by the branching nature of the fall salinity-*fDOM* relationship.

Fig. 4

a *fDOM* versus observed sea surface height (SSH) and **b** salinity at the Kirkpatrick Marsh Creek for the three time series in Fig. ~~4~~2

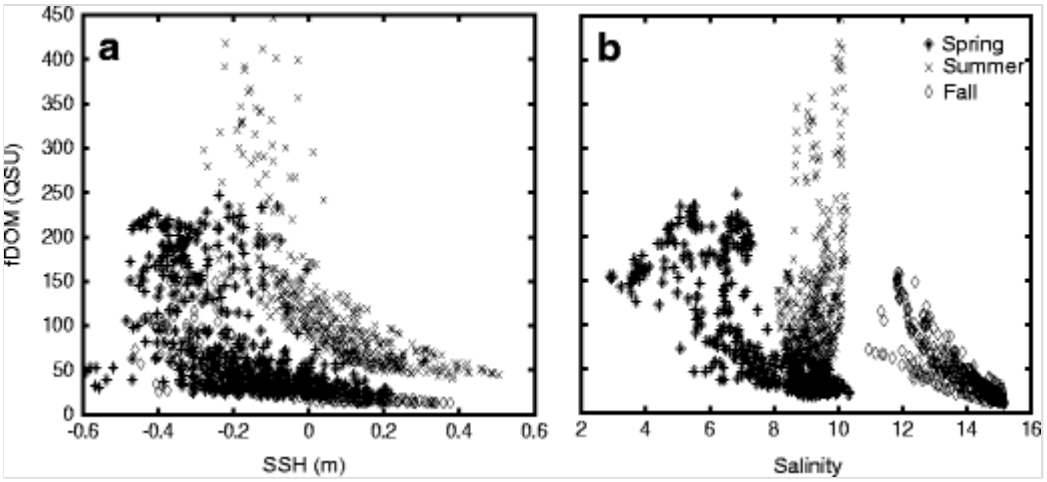

In the spring and fall, the salinity and *fDOM* negatively covaried consistently with a lag centered around 0 days, suggesting the variance of both were being driven by the same process (Table 3). The observed time series from August, however, exhibited a steadily increasing trend in salinity from approximately August 12 to August 22 followed by a complex pattern of high northwest wind velocity accompanied by an increase in salinity and spike in *fDOM* signal (Fig. 2b). This indicates the wind was driving the same physical mechanism associated with the *fDOM* signal intensity as observed in spring and fall because the pattern of covariance between wind and *fDOM* remained consistent. However, the covariance of *fDOM* and salinity was much weaker and had the opposite sign compared to the spring and fall (Fig. 3b; positive correlation), indicating that water that was released out of the wetland had a higher salinity than the outlying estuary. The August 21 storm event that was followed by a sharp increase in salinity appeared to be driven by wind forcing rather than an increase in freshwater discharge into the system from precipitation. In summer months during long dry periods, evaporation on the marsh surface can concentrate salinity in the marsh porewater (Correll 1981). As north winds accelerated around August 22nd, high salinity marsh water that was concentrated due to evaporation over the extended dry period from August 14–20 appeared to have been released from the marsh creek along with a large pulse of *fDOM*. The *fDOM* signal in summer fluctuated both positively and negatively with salinity with an overall higher magnitude of *fDOM* signal compared to the other seasons (see Fig. S1 in the Supplemental Materials for the full *fDOM* time series from 2015). The overall higher magnitude in *fDOM* signal in the summer

corresponds with observed seasonally higher DOC concentrations at the marsh creek in the summer and early fall months (Jordan et al. 1991; Tzortziou et al. 2008).

Storm events with both wind and precipitation clearly impacted both *fDOM* and salinity in the marsh creek, but it appears that wind velocity mediated freshwater transport and mixing as it entered the marsh-estuary system and determined the strength and direction of the salinity signal variation at the marsh creek. In most cases, large declines in salinity covaried with increases in *fDOM* and occurred independently of local rain events (dots in Fig. 2). This suggests that overland freshwater runoff potentially had some correlation to *fDOM* influx from the marsh to the estuary, but that wind driven inundation and mixing mediated the response in both the salinity and *fDOM* signal. Only when the winds were in a favorable direction for marsh outflow did the freshwater input show up as a decrease in salinity at the marsh creek.

For the entire EXO2 deployment (March 2015 through November 2015), *fDOM* had a negative covariance with N-S wind and weak positive covariance with E-W winds (Total, Table 3). Depth and *fDOM* were also tightly coupled; wind driven changes in SSH at the marsh creek coincided with changes in *fDOM*. As water elevation drops due to NW winds pushing water out of the Rhode River, marsh water is released from the marsh creek into the estuary. Salinity and *fDOM* also had a strong negative covariance throughout the time series centered at a lag of 1 h. The strong anti-correlation between *fDOM* and salinity and their variation with wind velocity indicates that both variables are related to wind forcing, primarily from the N-S component direction but secondarily from the E-W direction. The reasons for this are addressed with the hydrodynamic RhodeFVCOM model in the next section.

Baseline Model Validation

RhodeFVCOM tidal elevation (SSH; deviation from mean sea level) was validated at the node closest to NOAA Tides and Currents Annapolis, MD station (tidesandcurrents.-noaa.gov), and the SERC dock. At Annapolis, the

high-frequency pass filtered tidal elevation showed strong agreement for the amplitude and period with observations (RMSE = 5.25 cm, $r = 0.93$). Including the low-frequency variation, the model captured the overall patterns of tidal height well, although the model missed some of the variability associated with large storm and wind events (RMSE = 15.31 cm, $r = 0.63$). The model grid coarseness in the Annapolis area likely contributed to an underestimation of some of the shallow water tidal effects at this location, but Annapolis is the closest NOAA continuous tidal monitoring station to the study site with a known datum and therefore provided the best comparison. Modeled tidal elevation at the SERC dock exhibited similar variability as measured tidal elevation in both the high-frequency pass ($r = 0.85$) and unfiltered ($r = 0.53$) records for the entire modeled time period, adding confidence to the model simulation of shallow water tidally driven circulation in the Rhode River.

The majority of the temperature (RMSE = 1.71 °C, $r = 0.98$) and salinity variability (RMSE = 1.43, $r = 0.88$) in observations from the SERC dock was captured for the modeled period (Fig. 5). The high model skill of the RhodeFVCOM temperature and salinity solution added confidence that shallow water circulation in the Rhode River was simulated well. Two early fall cooling events where the magnitude of cooling was over predicted by the model contributed substantially to the error in the temperature solution. There was no observational data for comparison at the beginning of the model time period due to a lack of measurements taken at the dock. Some of the salinity draw down in the early spring and late fall was not captured with the model (see discussion).

Fig. 5

Modeled and observed **a** salinity ($r = 0.88$, RMSE = 1.43) and **b** temperature ($r = 0.98$, RMSE = 1.71 °C) at the SERC dock. Gaps in the observed data are periods when the sonde was removed for maintenance

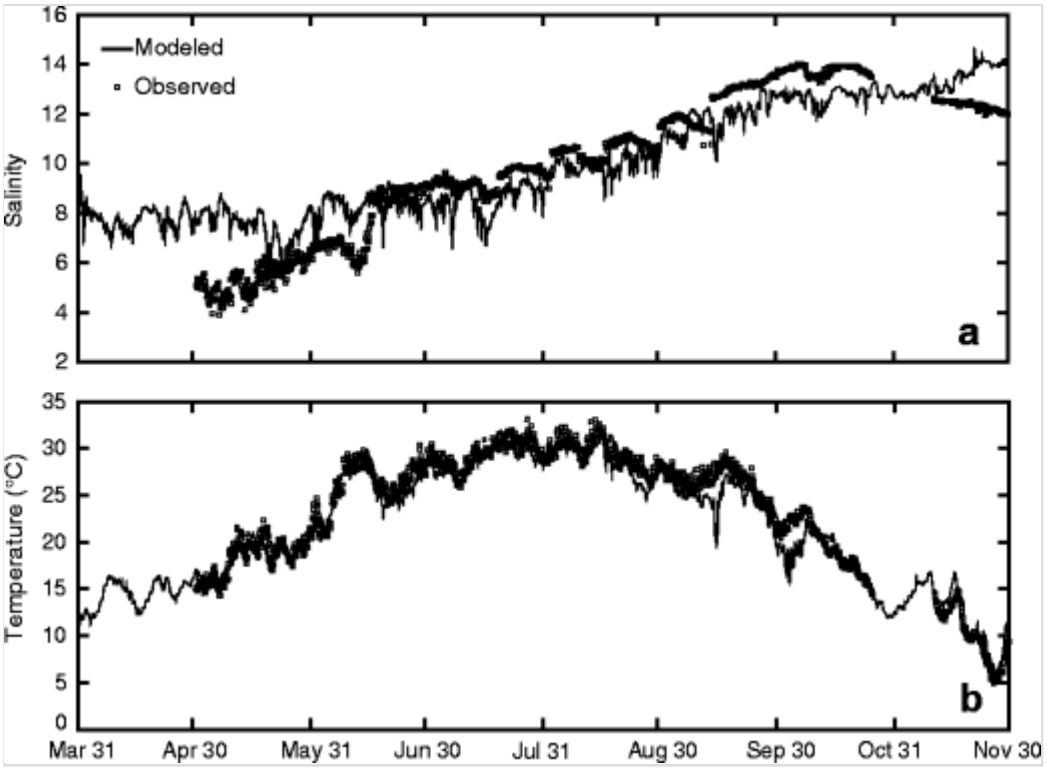

The inundated area of the marsh as a function of flooding tidal stage at the marsh creek (hypsometry; Eq. 2, following Jordan and Correll 1991) from the model is compared with data collected at semi-continuous frequency from June to August 2015 in Fig. 6. The inflection point of both scatter sets indicates the tidal stage at which the flooding water surface reaches the edge of the marsh creek bank. This represents the tidal height at which the marsh platform begins to flood. The inflection points of both modeled and observed hypsometry are similar, indicating the model marsh platform elevation was similar to the actual Kirkpatrick Marsh, although the model was ~10 cm less, which is due to the modeled creek depth being slightly shallower. The model predicted more area inundated, on average, but was of correct magnitude. The slope of the marsh hypsometric curve is steeper in the model, indicating RhodeFVCOM predicted a more rapid flooding of the marsh relative to observations. This happened because the modeled wetland bathymetry had a shallower slope compared to the real wetland. A shallower slope favors a conservative prediction of RhodeFVCOM outflow velocity because it reduces gravity driven flow in the model as the wetland is draining. Conversely, a modeled wetland with a steeper slope than the real marsh would favor an over prediction of the outflow velocity. The step function

nature of the modeled inundation curve can be attributed to the finite representation of the slope in the wetland area; each cell at each elevation is flooded instantaneously when D_{min} was exceeded. The entire wetland area was generally only flooded on spring tides.

Fig. 6

A hypsometric curve generated by RhodeFVCOM and calculated inundation area vs elevation from acoustic Doppler velocimetry (ADV) probe observations at the Kirkpatrick Marsh creek from June to December 2015. Inundation areas were calculated as the flow rate at the marsh creek ($m^3\ s^{-1}$) divided by the rate of tide stage change ($m\ s^{-1}$; Eq. 2). The modeled inundated area is the actual area of a sub-section of the marsh that RhodeFVCOM has predicted with a height above D_{min} (0.05 m) at each time step

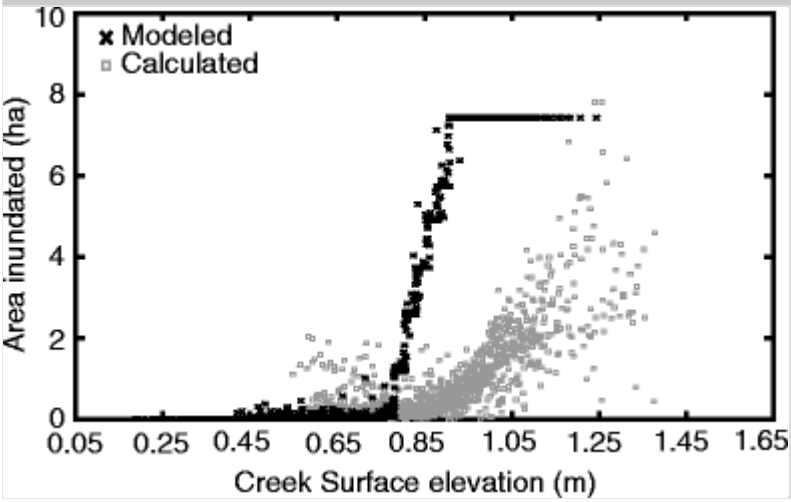

Velocity comparisons between model elements inside the marsh creek and 60 m adjacent on the marsh platform (dot in Fig. 1c) when there is greater than 10 cm of water depth at an adjacent model node offers insight into the effect of both bottom friction and marsh grass drag on the flow field. Depth and time averaged median horizontal flow velocity on the marsh platform ($1.29\ cm\ s^{-1}$) was substantially depressed relative to an element in the marsh creek, ($1.74\ cm\ s^{-1}$). In addition, runs without the marsh grass drag module resulted in a 3.0% increase in median horizontal surface velocity and a 9.9% increase in median vertical velocity for the same model element. In a model run without the marsh grass drag model, a similar decrease in horizontal

velocity from the marsh creek to a node on the marsh platform was also observed. This indicates that the majority of velocity reduction over the marsh platform appears to be independent of the presence or absence of vegetation and most of the velocity reduction is due to drag induced by the shallow flow over the marsh platform, in agreement with vegetation removal experiments (Leonard and Croft 2006). Leonard and Croft (2006) also found a substantial decrease in the vertical velocity component in the marsh interior, consistent with the findings in RhodeFVCOM.

AQ6

Atmospheric Forcing Sensitivity Experiments

Experimentally altering the wind direction during storm events in the model had a strong effect on the salinity variability at the marsh creek in the spring and early summer (Fig. 7). A southerly wind (test SW) during storms increased depth averaged salinity by 2.15 psu relative to the northerly storm wind (test NW) for the period of March 31 to July 19. The increased freshwater signal at the marsh creek in test NW was greatest in the early April storm events (Fig. 7). Low salinity water persisted at the marsh creek for multiple days and up to 2 weeks following a series of storm events. The response of the salinity signal for the two tests occurred before the peak discharge for both the early April and May 22 events (Fig. 7). This early salinity response is owed to the wind bracket around storm events in the model forcing. The wind started blowing either southerly (test SW, increased salinity) or northerly (test NW, decreased salinity) 24 h before the increased discharged. The wind set up the salinity signal before the freshwater discharge, further exhibiting the strong effect that wind had on the salinity at the marsh creek. A change in wind direction can drive a change in salinity independent of a large discharge event.

Fig. 7

a Modeled salinity in the Kirkpatrick marsh creek for the three numerical experiments and **b** interpolated river discharge forcing from the Muddy Creek watershed. Test SW is forced with wind from the south during storms, and test NW is forced with wind from the north during storms

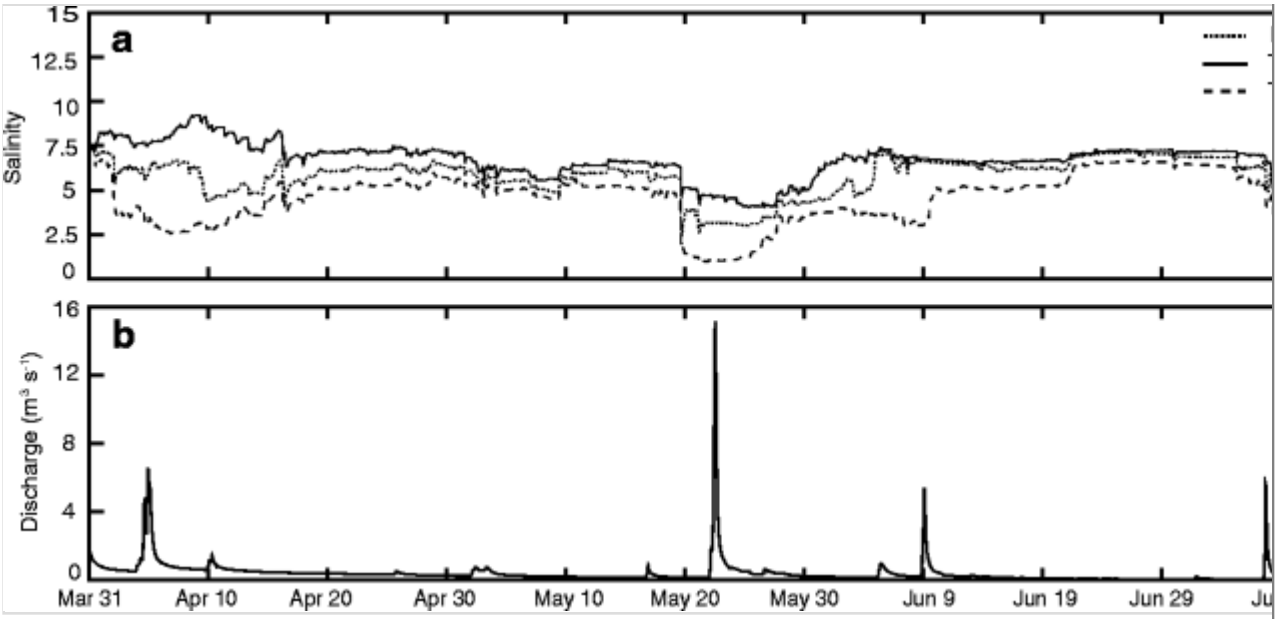

During the summer, the salinity remained generally the same across the three model runs. When storms did occur and the wind patterns were experimentally altered in the late summer and early fall (September–November; not shown), only a small difference in the salinity for each model run occurred. The wind effect was most pronounced in the spring when marsh creek salinity was lower and freshwater input into the system was highest. The strong salinity variation produced by altering the model wind direction corroborates that wind forcing was driving much of the salinity and anti-correlated *fDOM* variability in the measurements from in 2015.

The model results also reveal that altering the wind direction caused changes in the flow velocity at the marsh creek in early spring and summer (March 31–July 19, Fig. 8a). Flow velocity directed out of the marsh creek was consistently elevated at the onset of northerly storm events in test NW compared to southerly events during storm events in test SW. Moreover, the difference in flow velocity at the creek between test SW and NW occurred consistently with changes in salinity, i.e., increases in flow out of the marsh creek were associated with lower salinity and vice versa.

Fig. 8

a Modeled low-pass cutoff filtered (36 h frequency) marsh creek velocity and **b** sea surface height (SSH) gradient from Kirkpatrick Marsh creek to the opposite side of the Rhode River in spring and early summer. Positive velocity

is marsh water efflux, and a positive gradient indicates the water surface is sloping away from the marsh towards the mouth of the river. The *asterisks* indicate when modeled storm winds were applied. Test SW is forced with wind from the south during storms; test NW is forced with wind from the north during storms

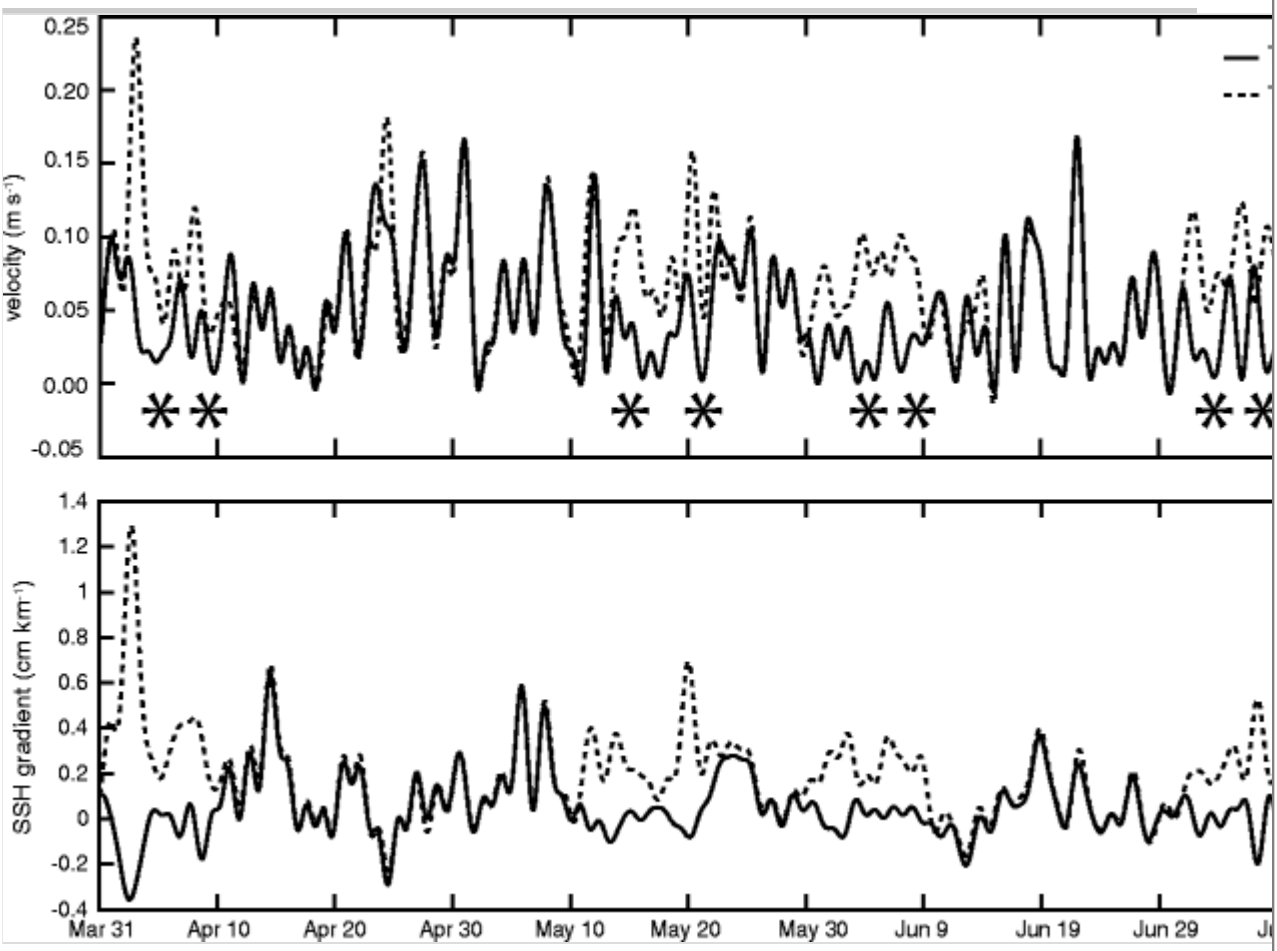

In the model experiments, changes in the wind velocity also caused changes in estuarine surface elevation in the Rhode River (Fig. 8b). The difference in surface elevation axially along the estuary during the northerly April storm event was >1.2 cm km^{-1} from the Kirkpatrick Marsh creek to the opposite side of the Rhode River. These changes in salinity, velocity, and surface elevation are consistent with the idea that northerly storm winds simultaneously drive water out of Muddy Creek into the estuary while also substantially pushing water out of the mouth of the river towards main stem Chesapeake Bay, setting up a pressure gradient sloping out of and away from the marsh creek. In contrast, it appears that southerly winds push water into

the mouth of the Rhode River from main stem Chesapeake Bay, causing water to accumulate opposite the wetland in the Rhode River, sloping back towards the marsh. It should be noted that two layer opposing flow was not consistently observed in the Rhode River model simulations and therefore likely does not greatly contribute to the mean flow.

ADV Observations

Limited observational data from a November 2015 ADV deployment allows a tentative corroboration of the modeled wind driven variability (Fig. 9). Northwest winds increased flow out of the marsh. Large *fDOM* pulses occurred during low water events. These pulses of *fDOM* are likely due to a combination of local wind-driven flow out of the Rhode River as predicted by the model and a drop in overall SSH of Chesapeake Bay, as confirmed by similarly low-pass filtered SSH data collected from Tolchester Beach, MD (not shown; tidesandcurents. noaa.gov). As the northwest winds relax, the pressure gradient set up by the wind leads to a “slosh” of water out of the marsh, likely enhancing export. The release of hydrostatic pressure on marsh porewater may also enhance porewater export that is high in CDOM into the tidal creek. The *fDOM* peaks in the observational data (e.g., between 11/14 and 11/16) occurred after the flow reversed out of the marsh creek. Estuarine water inflow initially diluted the high *fDOM* signal at the marsh creek, and upon wind relaxation and flow reversal, as hydrostatic pressure was released *fDOM* was released out of the wetland into the tidal creek. CDOM export during low water events is consistent with previously observed tidal dynamics of Kirkpatrick Marsh CDOM fluxes (Tzortziou et al. 2008).

Fig. 9

Low-pass filtered flow ($m^3\ s^{-1}$), deviation from mean water depth (m), and mean-normalized *fDOM* at the marsh creek. Negative flow is out of the marsh, positive is into the marsh

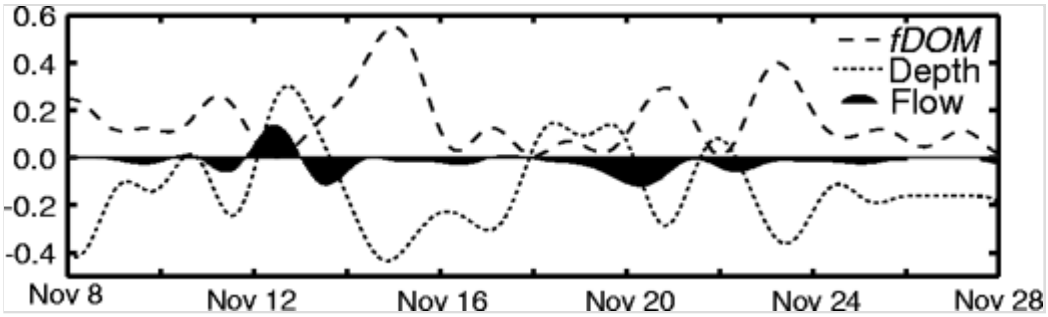

Discussion

Past studies have examined the effect that winds can have on marsh erosion and sediment transport (Dame et al. 1986; Stevenson et al. 1988) and compared fluxes of nutrients under differing measured wind regimes and topographically diverse salt marsh sites (Childers et al. 1993). In general, this study corroborates these past studies and previous qualitative estimates of wind-driven marsh tracer flux. Winds have an indirect local effect on the marsh water level, either enhancing or depressing marsh inundation at the onset of storm events and thus affecting marsh-estuary water exchange. In the Rhode River, as NW winds persist, flow out of the marsh is enhanced, primarily due to water being driven out of the mouth of the sub-estuary. The effect of wind on the estuarine pressure gradient explains much of the observed variability in both *fDOM* and salinity at the marsh creek (see conceptual diagram Fig. S2 in Supplemental Materials). The response of the Rhode River to N-S wind components is primarily related to the geographic orientation of the estuary. Therefore, consideration should be given for a particular wetland to the local response of that wetland to wind forcing.

Quantifying the input of both terrestrial and marsh biogeochemical end members into the estuary has implications for estuarine carbon cycling and productivity. Correll (1981) and Jordan et al. (1991) describe nutrient budgets for the Rhode River and Kirkpatrick Marsh, including freshwater runoff inputs. Correll (1981) notes that neglecting overland freshwater inputs can skew results towards overestimation of marsh biogeochemical transformations. The observations presented here show that wind affects how freshwater runoff from the watershed moves between the terrestrial, intertidal, and estuarine areas, having a direct effect on the marsh water and

fDOM export. The model experimental results corroborate these observations; wind largely determines how fresh and saline water mix at the marsh-estuary interface and likely has similar influence over other conservative and non-conservative tracers.

Observations show that during and following northwest wind events, strong pulses of *fDOM* are seen at the marsh creek. These signals are indicative of highly colored DOM, of which the marsh has been shown to be a source to the adjacent estuary across all seasons (Tzortziou et al. 2008, 2011). Model results show that the wind sets up a pressure gradient due to differences in water surface elevation across the Rhode River. In addition, the enhanced flow out of Muddy Creek during northerly wind events can also be a source of *fDOM* to the estuary and potentially contributes to the signal seen at the marsh creek. The magnitude of the pressure gradient is directly dependent on the direction, duration, and velocity of wind events. It appears that, as sustained northwesterly winds slacken, the pressure gradient sloping out of the marsh creek is released and large amplitude spikes in *fDOM* are observed (Fig. 2). Because of the sinuous and changing orientation of the river relative to the winds, northwest winds initially drive water back onto the marsh platform while also pushing water out of the mouth of the Rhode River into Chesapeake Bay, while southeasterly winds appear to have the opposite effect.

Large-scale (Bay-wide) circulation and SSH variability patterns that can contribute to the change in surface elevation at the marsh creek and in the Rhode River are not captured in the model. Main stem Chesapeake Bay circulation and SSH can be influenced by wind-driven events on both short (<4 days) and long time scales (Wang 1979b). Wang (1979a) found that E-W winds influence SSH across the bay on a time scale of 3–5 days, and N-S winds at a shorter time and space scale. This study, however, addresses the local forcing on a small tributary that appears to be important on shorter time scales (0–1 days), which is likely embedded in the larger regional atmospheric-driven SSH signal. The boundaries of RhodeFVCOM are forced with the model predicted SSH under normal atmospheric conditions. Therefore, in the experiments presented in this paper, larger-scale circulation effects are not captured. There is potentially a significant non-local effect

that enhances marsh water inflow and outflow during storm events in addition to the local forcing on the Rhode River demonstrated here. Additional future numerical manipulations utilizing a larger-scale regional model can be used to explore more non-local and regional impacts that wind-driven dynamics have on marsh water movements. Nonetheless, modeling results suggest that local wind forcing can cause sub-tidal flow variation between the wetland and estuary.

The optical, high-resolution measurements of *fDOM* from the EXO-2 probe at the marsh creek allowed the exploration of the sub-tidal variability of DOM across tidal, sub-tidal, and inter-seasonal time scales. *fDOM* spikes were consistently observed with pulses of lower salinity water, although the summer shows a decoupling between *fDOM* and salinity (Figs. 2, 3, and 4). The salinity and *fDOM* signals appeared to vary independently of precipitation events. Northerly winds following a sustained southerly wind event can drive large fluxes of *fDOM* out of the marsh, independent of season and precipitation. Winds masked the discharge of freshwater into the Rhode River often accompanying strong southwesterly winds. Furthermore, in the summer when marsh water would be expected to have an elevated salinity compared to the surrounding estuary due to evaporation on the wetland surface (Correll 1981), a northwesterly wind event was followed by an increase in salinity at the marsh creek co-occurring with a spike in *fDOM*. Elevated salinity in marsh water relative to the surrounding estuary during summer time could explain the positive relationship between *fDOM* and salinity seen on August 22nd. The branching nature of the *fDOM*-salinity cross-plots in both the spring and fall (Fig. 4) offers qualitative evidence of Muddy Creek water interacting with marsh-derived water at the marsh creek. Muddy Creek water would contribute *fDOM* to the estuary. Therefore, the combination of low salinity and high *fDOM* could represent mixing of marsh and Muddy Creek waters during northwesterly wind events accompanied by freshwater discharge. The contribution of each source to the overall signal is unclear, but previous studies have shown large amounts of export of *fDOM* at the marsh creek accompanying low water events (Tzortziou et al. 2008, 2011). The August 22nd event clearly shows that *fDOM* can be exported out of the marsh independent of freshwater input.

RhodeFVCOM captured the shallow water temperature and salinity variability well for the year 2005. The model, however, did not capture all of the variability, over-predicting the salinity in the late spring and fall. The missed salinity variability is potentially due to unresolved overland flow contributing to the salt balance. The high bank to estuary ratio suggests overland freshwater flow contribution may be important when freshwater input via precipitation is high (Correll 1981; Jordan and Correll 1991). Some of the watershed, including areas on the east side adjacent to the marsh, is outside of the measured area and was not included as freshwater input into the model domain. Including overland diffuse discharge points into the model may help drive the estuary salinity lower during spring and fall freshwater discharge events. Groundwater discharge likely also contributes to the freshwater input into the Rhode River (Jordan et al. 1991), but is currently not included in RhodeFVCOM.

Water column temperature is accurately predicted in the shallow water and main channel. Water column and sediment temperature variability has important implications for future biogeochemical simulations of the marsh-estuary ecosystem. The internally calculated heat flux algorithm used here is crucial to resolving the temperature as opposed to forcing the model with a specified net heat flux from atmospheric models, which is commonly done. The heat flux formulation factors in the balance between net short wave and long-wave radiation, with both contributing to the heating and cooling of the surface layer of the model. If either is incorrectly predicted, it will lead to inaccurate surface heat flux forcing and inaccurate FVCOM water temperature. NARR consistently over predicts net long-wave radiation flux (Kumar and Merwade 2011), and this problem is potentially exacerbated by the likely large amplitude variation in long-wave radiation that occurs in land-influenced estuarine NARR grid cells. As discussed above, a correction factor of 0.5 is applied to the NARR predicted net long-wave radiation flux in order to resolve the temperature in the summer.

Modeled flow velocity over the marsh platform was extremely reduced relative to the tidal creek. However, these velocity comparisons between model elements inside and outside of the wetland and model runs with and

without plant momentum drag in the marsh area are sensitive to the choice of the locations that are compared and the statistical approaches that are used to compare them. The microtidal environment in the Rhode River and the irregularity with which the Kirkpatrick Marsh is flooded offers an interesting comparison of the flow field from the marsh creek to the marsh interior, similar to observational studies (e.g., Christiansen et al. 2000; Leonard and Croft 2006). Marsh water depth is consistently low, exceeding 10 cm in surface elevation only 11% of the time at the selected marsh node used for comparison (Fig. 1c). Pairwise (20.7% velocity reduction) vs unpaired (25.7% velocity reduction) comparisons of the velocity time series of flow in the marsh creek versus the marsh interior gave different results, although similar conclusions. Comparing flow in the creek and on the wetland surface for all model time points (n = 5808) produces a median velocity reduction of 85.4% from the creek to the marsh interior. Rather, there is a 25.7% velocity reduction if instead times when the wetland is flooded to a depth greater than 10 cm (n = 656) are compared. Spatial heterogeneity in the marsh platform flow field can produce strongly differing velocity, depending on the model output location and frequency. Thus, careful consideration is needed in both observational and modeling comparisons to accurately quantify the relative contribution of surface friction and drag induced by marsh grass stems. Nonetheless, the hydrology in the wetland is reasonably recreated in the model and the drag model in RhodeFVCOM allows future studies to assess how the inclusion of explicit marsh plants in wetland areas affects biogeochemical processes and residence time.

The slope of the modeled hypsometric plot indicates the model overestimates the rate at which the marsh floods relative to observations taken in 2015, which is indicative of a shallower slope in the modeled marsh surface relative to the Kirkpatrick Marsh (Fig. 6). The differences between modeled and calculated curves appear to be due to a modeled depth that is shallower on average, which gives rise to the difference in the inflection point, combined with substantially less variance in the model output which is inherent in a deterministic model. Even though the maximum area inundated predicted by RhodeFVCOM is greater than the calculated area inundated, because the slope of the modeled bathymetry in the wetland is less than

observed, the model is potentially underestimating flow velocity out of the wetland creek because there is a weaker hydrostatic pressure gradient for any two points across the wetland surface. The total volume that passes through the creek during a given tidal cycle would be greater, however, which could lead to an overestimation of wetland discharge. Calculated hypsometry is an estimate of inundation based on the relationship between marsh creek flow and change in tidal stage (Eq. 2). Inherent in the hypsometric estimation from observations at the marsh creek is the assumption that the marsh region in question is only flooded through the tidal creek, which could potentially lead to an under prediction of the inundated area if there is over-edge sheet flow. The model analysis, however, recorded when every marsh grid cell in the area that was deemed to potentially drain the tidal creek has a surface water elevation >0.055 m, which is independent of the source of the water in the marsh grid cell. The delineation between modeled wetland areas affected the maximum area inundated because if a larger potential inundation area was used in the model analysis, then it would appear that the model is more flooded relative to the observations on any given tide. In addition, some of the difference between modeled and observed inundation from RhodeFVCOM arises from predicted intermittent sheet flow over the marsh edge onto the platform during flood tides. Over edge marsh flooding in the model appears to be related to wind forcing driving water into the back of the tributary, runoff from Muddy Creek, and spring tides. More work is needed to quantify the variability of marsh platform flooding, including the delineation of each region within the marsh, in order to resolve the differences in modeled and observed inundation progression and rate.

It should be stressed that each wetland's response to differential wind forcing will be determined by that wetlands orientation in relation to dominant wind forcing patterns. Indeed, there may be a dynamic relationship between dominant wind patterns for a certain region and the likelihood of a wetland to export large amounts of *fDOM*. Although this study did not look directly at wetland erosion/deposition, the relationship between those processes and inundation patterns would also likely be influenced by wind similarly to *fDOM* and salinity.

Conclusion

Modeled marsh-estuary water flow is influenced by sub-tidal variability of wind-driven estuarine water surface elevation in the Rhode River, MD. Observed wind-driven *fDOM* variability is consistent across the seasons, showing the influence that atmospheric forcing has on marsh DOM efflux. The wind-driven setup of pressure gradients can dominate the tidal signal, exerting a strong control on the water exchange across the marsh-estuary interface. Water flow and inundation ultimately govern the timing and magnitude of biogeochemical exchanges and processes between the marsh and estuary. The modeling exercises allow exploration of how different physical phenomena affect the inundation regime, hypsometry, and marsh water residence time on the marsh platform. By varying wind forcing and modeled vegetation characteristics, in addition to bathymetry, RhodeFVCOM can be used as a tool to study how different factors influence the flow across the marsh-estuary interface. Marsh water residence time has been demonstrated to have strong control over many wetland processes (e.g., Childers et al. 1993; Bockelmann et al. 2002); therefore, it cannot be ignored in any realistic wetland hydrodynamic modeling application.

Modeling of the Rhode River can capture the local effect of wind and allow a detailed analysis that would otherwise be difficult to empirically measure. Ongoing studies are utilizing the hydrodynamic modeling results to drive a biogeochemical model to further explore marsh-estuary dissolved organic carbon cycling. As understanding of the physical drivers of marsh water exchange broadens, improved models will help foster predictions for future changes in tidal wetland-estuary carbon cycling. Quantifying the physical controls on marsh DOM processes will help reduce the uncertainty that still exists on the role wetlands play in estuarine and coastal ocean carbon cycling.

Acknowledgements

We would like to thank Andrew Peresta for deploying and maintaining the EXO2 sonde at the Kirkpatrick Marsh creek and the entire MARSHCYCLE team for many thoughtful discussions. We would also like to thank two anonymous reviewers for comments that helped greatly improve this manuscript. This research was supported by National Aeronautics and Space

Administration grant NNH13ZDA001N-CARBON. Contact the corresponding author for model forcing and output and post processing scripts.This is University of Maryland Center for Environmental Science contribution # 5392.

Electronic supplementary material

Fig. S1

(a) Unfiltered *fDOM* and (b) depth for the entire sampling period in 2015. Gaps in the data indicate periods when the EXO-2 Sonde was not deployed. (DOCX 110 kb)

Fig. S2

Conceptual diagram of the estuarine surface gradient progression during a "typical" wind progression in the Rhode River, MD in the spring and fall. As southerly winds blow a barotropic surface pressure gradient sets up in the back of the Rhode River depicted by the H in (a) that forces water back towards the marsh, depressing flow out of the wetland depicted by the shaded region. As Northwesterly winds progress, local wind driven flow enhances flow out of the creek back towards the marsh, while local wind effects set up a low pressure in the back and mouth of the Rhode River, depicted by the L's (b). (DOCX 145 kb)

References

AQ7

Blumberg, Alan F., and David M. Goodrich. 1990. Modeling of wind-induced destratification in Chesapeake Bay. *Estuaries* 13.3: 236–249.

Bockelmann, Anna C., Jan P. Bakker, Reimert Neuhaus, and Jochim Lage. 2002. The relation between vegetation zonation, elevation and inundation frequency in a Wadden Sea salt marsh. *Aquatic Botany* 73.3: 211–221.

Breitburg, D. L., A. H. Hines, T. E. Jordan, M. K. McCormick, D. E.

Weller, and D. F. Whigham. 2008. Landscape patterns, nutrient discharges, and biota of the Rhode River estuary and its watershed: Contribution of the Smithsonian Environmental Research Center to the Pilot Integrated Ecosystem Assessment. Smithsonian Environmental Research Center, Edgewater, Maryland.

Bridgham, Scott D., J. Patrick Megonigal, Jason K. Keller, Norman B. Bliss, and Carl Trettin. 2006. The carbon balance of North American wetlands. *Wetlands* 26.4: 889–916.

Chen, Changsheng, Hedong Liu, and Robert C. Beardsley. 2003. An unstructured grid, finite-volume, three-dimensional, primitive equations ocean model: application to coastal ocean and estuaries. *Journal of Atmospheric and Oceanic Technology* 20.1: 159–186.

Chen, Changsheng, Jianhua Qi, Chunyan Li, Robert C. Beardsley, Huichan Lin, Randy Walker, and Keith Gates. 2008. Complexity of the flooding/drying process in an estuarine tidal-creek salt-marsh system: An application of FVCOM. Journal of Geophysical Research: Oceans 113.C7.

Chen, C., Beardsley, R.C., Cowles, G., Qi, J., Lai, Z., Gao, G., Stuebe, D., Liu, H., Xu, Q., Xue, P. and Ge, J., 2013. An unstructured-grid, finite-volume community ocean model FVCOM User Manual. SMAST-UMASSD Technical Report-13-0701, University of Massachusetts-Dartmouth. 37–44.

Childers, Daniel L., Stephen Cofer-Shabica, and L. Nakashima. 1993. Spatial and temporal variability in marsh-water column interactions in a southeastern USA salt marsh estuary. *Marine Ecology Progress Series* 95.1-2: 25–38.

Chmura, Gail L., Shimon C. Anisfeld, Donald R. Cahoon, and James C. Lynch. 2003. Global carbon sequestration in tidal, saline wetland soils. Global biogeochemical cycles 17.4.

Christiansen, T., P.L. Wiberg, and T.G. Milligan. 2000. Flow and sediment transport on a tidal salt marsh surface. *Estuarine, Coastal and Shelf Science.* 50.3: 315–331.

Correll, David L. 1981. Nutrient mass balances for the watershed, headwaters intertidal zone, and basin of the Rhode River estuary. *Limnology and Oceanography* 26.6: 1142–1149.

Dame, R., T. Chrzanowski, K. Bildstein, B. Kjerfve, H. McKellar, D. Nelson, J. Spurrier, S. Stancyk, H. Stevenson, J. Vernberg, and R. Zingmark. 1986. The outwelling hypothesis and North inlet, South Carolina. *Marine Ecology Progress Series* 33.2: 217–229.

Del Vecchio, Rossana, and Neil V. Blough. 2002. Photobleaching of chromophoric dissolved organic matter in natural waters: kinetics and modeling. *Marine Chemistry* 78.4: 231–253.

Downing, Bryan D., Brian A. Pellerin, Brian A. Bergamaschi, John Franco Saraceno, and Tamara E.C. Kraus. 2012. Seeing the light: The effects of particles, dissolved materials, and temperature on in situ measurements of DOM fluorescence in rivers and streams. *Limnology and Oceanography: Methods* 10.10: 767–775.

Fagherazzi, Sergio, Patricia L. Wiberg, Stijn Temmerman, Eric Struyf, Yong Zhao, and Peter A. Raymond. 2013. Fluxes of water, sediments, and biogeochemical compounds in salt marshes. *Ecological Processes* 2.1: 1–16.

Fairall, Chris W., Edward F. Bradley, David P. Rogers, James Bearer Edson, and George S. Young. 1996. Bulk parameterization of air-sea fluxes for tropical ocean-global atmosphere coupled-ocean atmosphere response experiment. *Journal of Geophysical Research: Oceans* 101.C2: 3747–3764.

~~Fichot, Cédric G., and Ronald Benner. 2011. A novel method to estimate DOC concentrations from CDOM absorption coefficients in coastal~~

~~waters. Geophysical Research Letters 38.3.~~

Geyer, W.R. 1996. Influence of wind on dynamics and flushing of shallow estuaries. *Estuarine, Coastal and Shelf Science* 44.6: 713–722.

Haddad, Jana, Seth Lawler, and Celso M. Ferreira. 2016. Assessing the relevance of wetlands for storm surge protection: a coupled hydrodynamic and geospatial framework. *Natural Hazards* 80.2: 839–861.

Herrmann, Maria, Raymond G. Najjar, W. Michael Kemp, Richard B. Alexander, Elizabeth W. Boyer, Wei-Jun Cai, Peter C. Griffith, Kevin D. Kroeger, S. Leigh McCallister, and Richard A. Smith. 2015. Net ecosystem production and organic carbon balance of US East Coast estuaries: a synthesis approach. *Global Biogeochemical Cycles* 29.1: 96–111.

Ikegami, M., D. F. Whigham, and M. J. A. Werger. 2006. *Scirpus olneyi* (Cyperaceae) shows phenotypical differentiation in a salt marsh on the east coast of the USA. Polish Botanical Studies.

Jordan, Thomas E., and David L. Correll. 1991. Continuous automated sampling of tidal exchanges of nutrients by brackish marshes. *Estuarine, Coastal and Shelf Science* 32.6: 527–545.

Jordan, Thomas E., David L. Correll, Joseph Miklas, and Donald E. Weller. 1991. Nutrients and chlorophyll at the interface of a watershed and an estuary. *Limnology and Oceanography* 36.2: 251–267.

~~Kim, Taeyun, and Tarang Khangaonkar. 2012. An offline unstructured biogeochemical model (UBM) for complex estuarine and coastal environments. *Environmental Modelling & Software* 31: 47–63.~~

~~Kim, Daehyun, William E. Grant, David M. Cairns, and Jesper Bartholdy. 2013. Effects of the North Atlantic oscillation and wind waves on salt marsh dynamics in the Danish Wadden Sea: a quantitative model as proof of concept. *Geo-Marine Letters* 33.4: 253–261.~~

Kumar, Sanjiv, and Venkatesh Merwade. 2011. Evaluation of NARR and CLM3. 5 outputs for surface water and energy budgets in the Mississippi River Basin. *Journal of Geophysical Research: Atmospheres* 116: D8.

Large, W.G., and S. Pond. 1981. Open ocean momentum flux measurements in moderate to strong winds. *Journal of Physical Oceanography* 11.3: 324–336.

Leonard, Lynn A., and Alexander L. Croft. 2006. The effect of standing biomass on flow velocity and turbulence in Spartina alterniflora canopies. *Estuarine, Coastal and Shelf Science* 69.3: 325–336.

Lu, Yuehan, James E. Bauer, Elizabeth A. Canuel, Yamashita Youhei, R.M. Chambers, and Rudolf Jaffé. 2013. Photochemical and microbial alteration of dissolved organic matter in temperate headwater streams associated with different land use. *Journal of Geophysical Research: Biogeosciences* 118.2: 566–580.

~~Mannino, Antonio, Mary E. Russ, and Stanford B. Hooker. 2008. Algorithm development and validation for satellite-derived distributions of DOC and CDOM in the US Middle Atlantic Bight. Journal of Geophysical Research: Oceans 113.C7.~~

~~Mannino, Antonio, Sergio Signorini, Michael Novak, John Wilkin, Marjorie AM Friedrichs, and Raymond G. Najjar. 2015. Dissolved organic carbon fluxes in the Middle Atlantic Bight: an integrated approach based on satellite data and ocean model products. Journal of Geophysical Research: Biogeosciences.~~

MATLAB. n.d. Statistics Toolbox and Signal Processing Toolbox, Release R2014B, The MathWorks, Inc., Natick, Massachusetts, United States.

Megonigal, J. Patrick, and Scott C. Neubauer. 2009. *Biogeochemistry of tidal freshwater wetlands. Coastal wetlands: an integrated ecosystem approach*, 535–562. Amsterdam: Elsevier.

Miller, William L., Mary Ann Moran, Wade M. Sheldon, Richard G. Zepp, and Stephen Opsahl. 2002. Determination of apparent quantum yield spectra for the formation of biologically labile photoproducts. *Limnology and Oceanography* 47.2: 343–352.

Moran, Mary Ann, Wade M. Sheldon, and Richard G. Zepp. 2000. Carbon loss and optical property changes during long-term photochemical and biological degradation of estuarine dissolved organic matter. *Limnology and Oceanography* 45.6: 1254–1264.

National Centers for Environmental Prediction/National Weather Service/NOAA/U.S. n.d. Department of Commerce. 2005, updated monthly. NCEP North American Regional Reanalysis (NARR). Research Data Archive at the National Center for Atmospheric Research, Computational and Information Systems Laboratory. http://rda.ucar.edu /datasets/ds608.0/ . Accessed 6 April, 2016.

Nepf, H.M. 1999. Drag, turbulence, and diffusion in flow through emergent vegetation. *Water Resources Research* 35.2: 479–489.

Nixon, Scott W. 1980. Between coastal marshes and coastal waters—a review of twenty years of speculation and research on the role of salt marshes in estuarine productivity and water chemistry. Springer US.

NOAA Tides and Currents. n.d. https://tidesandcurrents.noaa.gov/ . Accessed 6 April, 2016.

R Core Team 2015. R: A language and environment for statistical computing. R Foundation for Statistical Computing, Vienna, Austria. URL http://www.R-project.org/ .

Rasse, Daniel P., Gary Peresta, and Bert G. Drake. 2005. Seventeen years of elevated CO2 exposure in a Chesapeake Bay wetland: sustained but contrasting responses of plant growth and CO2 uptake. *Global Change Biology* 11.3: 369–377.

Schubel, J.R., and D.W. Pritchard. 1986. Responses of upper Chesapeake Bay to variations in discharge of the Susquehanna River. *Estuaries* 9.4: 236–249.

~~Scully, Malcolm E. 2010. Wind modulation of dissolved oxygen in Chesapeake Bay. *Estuaries and Coasts* 33.5: 1164–1175.~~

Scully, Malcolm E., Carl Friedrichs, and John Brubaker. 2005. Control of estuarine stratification and mixing by wind-induced straining of the estuarine density field. *Estuaries* 28.3: 321–326.

Sherwood, Chris. 1989 Revised by P. Wiberg, 2003. MATLAB function lpfilt. The MathWorks Inc., Natick, Massachusetts, United States.
AQ8

Stevenson, J. Court, Larry G. Ward, and Michael S. Kearney. 1988. Sediment transport and trapping in marsh systems: implications of tidal flux studies. *Marine Geology* 80.1: 37–59.

Sulzberger, Barbara, and Edith Durisch-Kaiser. 2009. Chemical characterization of dissolved organic matter (DOM): a prerequisite for understanding UV-induced changes of DOM absorption properties and bioavailability. *Aquatic Sciences* 71.2: 104–126.

Teal, John M. 1962. Energy flow in the salt marsh ecosystem of Georgia. *Ecology* 43.4: 614–624.

~~Temmerman, Stijn, G. Govers, P. Meire, and S. Wartel. 2003. Modelling long-term tidal marsh growth under changing tidal conditions and suspended sediment concentrations, Scheldt estuary, Belgium. *Marine Geology* 193.1–2: 151–169.~~

Trapletti, Adrian and Kurt Hornik 2015. tseries: time series analysis and computational finance. R package version 0.10–34.

Twardowski, Michael S., Emmanuel Boss, James M. Sullivan, and Percy

L. Donaghay. 2004. Modeling the spectral shape of absorption by chromophoric dissolved organic matter. *Marine Chemistry* 89.1: 69–88.

Tzortziou, Maria, Christopher L. Osburn, and Patrick J. Neale. 2007. Photobleaching of dissolved organic material from a tidal marsh-estuarine system of the Chesapeake Bay. *Photochemistry and Photobiology* 83.4: 782–792.

Tzortziou, Maria, Patrick J. Neale, Christopher L. Osburn, J. Patrick Megonigal, Nagamitsu Maie, and Rudolf Jaffé. 2008. Tidal marshes as a source of optically and chemically distinctive colored dissolved organic matter in the Chesapeake Bay. *Limnology and Oceanography* 53.1: 148–159.

Tzortziou, Maria, Patrick J. Neale, J. Patrick Megonigal, Crystal Lee Pow, and Megan Butterworth. 2011. Spatial gradients in dissolved carbon due to tidal marsh outwelling into a Chesapeake Bay estuary. *Marine Ecology Progress Series* 426: 41–56.

Vinnikov, Konstantin. 2015. Baltimore – Washington Airport Wjind Climatology. http://www.atmos.umd.edu/~kostya/NIST/WIND/SURFACE/KBWI_2010_10or13_WIND_2.pdf . Accessed March 8, 2017.

Wang, D.P. 1979a. Subtidal sea level variations in the Chesapeake Bay and relations to atmospheric forcing. *Journal of Physical Oceanography.* 9.2: 413–421.

Wang, D.P. 1979b. Wind-driven circulation in the Chesapeake Bay, winter, 1975. *Journal of Physical Oceanography.* 9: 564–572.

Wang, Zhaohui Aleck, and Wei-Jun Cai. 2004. Carbon dioxide degassing and inorganic carbon export from a marsh-dominated estuary (the Duplin River): A marsh CO2 pump. *Limnology and Oceanography* 49.2: 341– 354.

AQ9

Wang, Taiping, Tarang Khangaonkar, Wen Long, and Gary Gill. 2014. Development of a kelp-type structure module in a coastal ocean model to assess the hydrodynamic impact of seawater uranium extraction technology. *Journal of Marine Science and Engineering* 2.1: 81–92.

Weather Underground. n.d. https://www.wunderground.com/us/md/annapolis . Accessed 6 April 2016.

Xu, Jiangtao, Wen Long, Jerry D. Wiggert, Lyon W.J. Lanerolle, Christopher W. Brown, Raghu Murtugudde, and Raleigh R. Hood. 2012. Climate forcing and salinity variability in Chesapeake Bay, USA. *Estuaries and Coasts.* 35.1: 237–261.

RF Dame, JD Spurrier, TM Williams, B Kjerfve, RG Zingmark, TG Wolaver, TH Chrzanowski, HN McKellar, FJ Vernberg, (1991) Annual material processing by a salt marsh-estuarine basin in South Carolina, USA. Marine Ecology Progress Series 72:153-166

Craig A. Stow, Jason Jolliff, Dennis J. McGillicuddy, Scott C. Doney, J. Icarus Allen, Marjorie A.M. Friedrichs, Kenneth A. Rose, Philip Wallhead, (2009) Skill assessment for coupled biological/physical models of marine systems. Journal of Marine Systems 76 (1-2):4-15